

Hot Jupiters in Old Wide-Binary Systems

Evgeni Grishin^{1,2}, Jet Winter¹, Jaime A. Alvarado-Montes^{3,4,5}

¹School of Physics and Astronomy, Monash University, Clayton, VIC 3800, Australia.

²OzGrav: Australian Research Council Centre of Excellence for Gravitational Wave Discovery, Clayton, VIC 3800, Australia.

³Australian Astronomical Optics, Macquarie University, Sydney, NSW 2109, Australia.

⁴Astrophysics and Space Technologies Research Centre, Macquarie University, Sydney, NSW 2109, Australia.

⁵Macquarie University Research Fellow (MQRF).

Contributing authors: evgeni.grishin@monash.edu;

Abstract

Hot Jupiters (HJs) are giant planets with orbital periods shorter than 10 days, found around $\sim 0.5\text{--}1\%$ of Sun-like stars [1]. Their origins remain debated despite decades of study [2]. The high prevalence of stellar companions [3], the eccentricity distribution of ‘Cold’ Jupiters on longer orbits [4], and the wide range of stellar spin–orbit misalignments [5] support high-eccentricity migration: planets are excited to eccentric orbits and subsequently circularised via tidal dissipation [6]. Existing high-eccentricity migration models, however, are inefficient in converting the initial population of Cold Jupiters to HJs. Current models reproduce at most $\lesssim 30\%$ of observed HJs [7], while the resulting Cold/Hot Jupiter ratios ($\gtrsim 30$) overproduce the observed values of 10–15 [8]. These models also fail to form HJs around old stars ($\gtrsim 3$ Gyr) on short tidal decay timescales (e.g., < 40 Myr [9]). Here we show that wide binaries ($a > 10^3$ au) perturbed by the Galactic tidal field produce 1.8 ± 0.14 more HJs compared to isolated binary systems, accounting for 26–40% of the observed population under conservative assumptions. Wide-binaries predominantly produce Gyr-old systems, consistent with the host-age distribution for $t \geq 2.5$ Gyr [10]. In $\sim 20\%$ of cases, wide-binary perturbations eject giant planets entirely, resolving the Cold/Hot Jupiter ratio discrepancy while naturally seeding the population of free-floating giant planets [11]. In our dynamical framework, wide binaries emerge as active agents that reshape planetary demographics across billions of years. These results will be decisively tested by forthcoming exoplanet and microlensing surveys.

Since the discovery of 51 Pegasi b [12], hundreds of Hot Jupiters (HJ) have been identified. These giant planets with masses $\gtrsim 0.3 M_J$ and orbital periods under 10 days form an almost complete magnitude-limited sample around FGK stars [13], with an occurrence rate of 0.5–1% [1]. Measurements of over 200 obliquity angles between the stellar spin and the HJ orbital plane via the Rossiter–McLaughlin (RM) effect [14] reveal a striking trend: hot host stars ($T_{\text{eff}} \gtrsim 6300$ K) exhibit random obliquities, while cool exoplanet hosts show predominantly aligned orbits [5]. This pattern supports high-eccentricity migration over disc migration or in-situ formation, with subsequent tidal alignment occurring efficiently in cool stars with convective envelopes, but inefficiently in hot stars with radiative envelopes. Moreover, the eccentricity distribution of Cold Jupiters aligns with expectations from high-eccentricity tidal migration [4]. In this scenario, the proto-HJ’s eccentricity is first excited—either by planet–planet scattering [15] or von Zeipel–Lidov–Kozai (ZLK) oscillations [16] driven by stellar companions [17]—and then tidally circularised at pericentre. Also, the binary fraction among HJ hosts is $\sim 50\%$ [18], significantly higher than the $\sim 20\%$ fraction in the general solar-type star population [19], thus preferring the ZLK migration pathway.

Extensive observational data support high-e migration, but current population models account for at most 15–30% of the observed HJ population [7, 20, 21]. The ZLK mechanism requires a narrow range of mutual inclinations, ι_{mut} , between the planetary and the stellar orbital planes, leaving behind a large population of “Cold Jupiters” ($a > 1$ au), with predicted Cold/Hot Jupiter ratios $\gtrsim 30$, well above the observed ratios of 10–15 [22]. A further challenge is the presence of HJs around old stars, in some cases with measured tidal decay times much shorter than their host’s age, such as NGTS-10 [9] with $t_{\text{age}} = 10.4 \pm 2.5$ Gyr and disruption time $\lesssim 40$ Myr [23]. These constraints suggest that many HJs must form relatively late. Chen et al. (2023) [10] found that while HJ occurrence declines modestly with age, a substantial fraction persist around stars older than $\gtrsim 5$ Gyr, with $\sim 50\%$ forming after 3 Gyr—incompatible with standard ZLK tidal migration. Recent astrometric data from Gaia has revealed millions of binaries [24] and $\sim 10^4$ hierarchical triples [25]. We demonstrate that the effects of Galactic tides (GT) on wide binaries ($a \gtrsim 10^3$ au) raise HJ occurrence rates by a factor of 1.8 ± 0.14 to $\sim 40\%$ of the observed rate, resolving the Cold/Hot Jupiter ratio tension and reproducing the observed host age distribution for $t \gtrsim 2.5$ Gyr. This makes wide-binary interactions a leading channel for old HJ systems and, potentially, the dominant channel for overall HJ formation.

Chaotic and secular dynamics of wide binary systems

Figure 1 sketches the wide binary orbit with typical separation $a_2 \gtrsim 10^3$ au inclined with an angle ι_{out} to the Galactic plane. One of the stars has a giant planet at an orbital semi-major axis $a_1 \gtrsim 5$ au. The mutual inclination between the two orbits is ι_{mut} . GT can make outer orbits undergo eccentricity oscillations similar to ZLK oscillations, originally applied for studying Sun-grazing Oort-cloud comets [26]. For a binary with separation a_2 and masses m_1 and m_2 , the timescale of such oscillations is

$$t_{\text{GT}} \approx 0.89 \left(\frac{m_1 + m_2}{M_{\odot}} \right)^{1/2} \left(\frac{a}{10^4 \text{ au}} \right)^{-3/2} \text{ Gyr.} \quad (1)$$

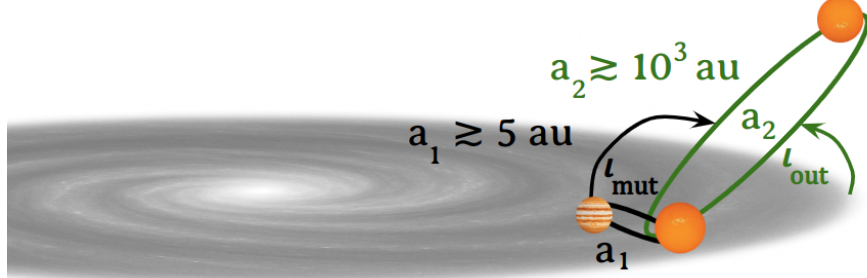


Fig. 1 Hierarchical wide three-body system of the two stars in a wide orbit (green ellipse) of semi-major a_2 , typically above 10^3 au. The outer wide binary star orbit is inclined with the galactic plane by an angle i_{out} . An inner binary giant planet (black ellipse) with semi-major axis $a_1 \gtrsim 5$ au. The mutual inclination between the orbits is i_{mut} .

The maximum eccentricity for the wide binary is $e_{2,\text{max}} = (1 - (5/4) \cos^2 i_{\text{out}})^{1/2}$. This can affect the timescale of the inner ZLK oscillations. The qualitative evolution is characterized by the ratio of the secular timescale to the GT timescale [27]

$$\mathcal{R}_0 = \frac{t_{\text{sec}}}{t_{\text{GT}}} \approx 1 \left(\frac{M_{\odot}}{m_2} \right)^{-1} \sqrt{\frac{2m_1}{m_1 + m_2}} \left(\frac{a_1}{25 \text{ au}} \right)^{-3/2} \left(\frac{a_2}{10^4 \text{ au}} \right)^{9/2} (1 - e_2^2)^{3/2}. \quad (2)$$

When \mathcal{R}_0 is of order unity, overlapping secular resonances lead the system to evolve chaotically, allowing the planetary orbit to attain extreme eccentricities [28].

Figure 2 shows the evolution of different examples of both regular and chaotic orbits. Regular orbits must start from small values of $\cos i_{\text{mut}}$ in order to effectively develop large eccentricities and form a HJ (a). In contrast, chaotic orbits can begin with any mutual inclination and evolve chaotically (b). In the case of regular orbits, tidal dissipation is gradual and occurs at a fixed pericentre $q_1 = a_1(1 - e_1)$. Several ZLK cycles are required to reduce the semi-major axis, consistent with the standard ZLK tidal migration channel [6] (c). Chaotic orbits evolve more erratically, with most of the tidal dissipation occurring once the pericentre crosses a certain threshold (d). The eccentricity e_1 undergoes periodic oscillations until tidal decoupling occurs. The outer eccentricity e_2 remains nearly constant for regular orbits (e). However, in the case of chaotic orbits, e_2 exhibits several periodic oscillations, causing the inner eccentricity e_1 to vary erratically. Efficient tidal dissipation takes place when e_1 reaches extreme values ($e_1 \approx 0.999$). The formation timescales can also distinguish the two channels: while regular orbits form HJs within ~ 1 Gyr, chaotic orbits evolve much more slowly on the order of ~ 10 Gyr.

Results of the population study

We set up a Monte-Carlo simulation with 10^4 initial conditions, split evenly between cases with GT turned on and off. Stellar masses are sampled from the Kroupa mass function between $0.5 - 1.5 M_{\odot}$, whereas the planet mass is fixed at $1 M_{\text{J}}$. Orbital separations are drawn from log-uniform distributions: $a_1 \sim \log U [5, 200]$ au and $a_2 \sim \log U [300, 3 \times 10^4]$ au, ensuring dynamical stability [29]. Mutual inclinations

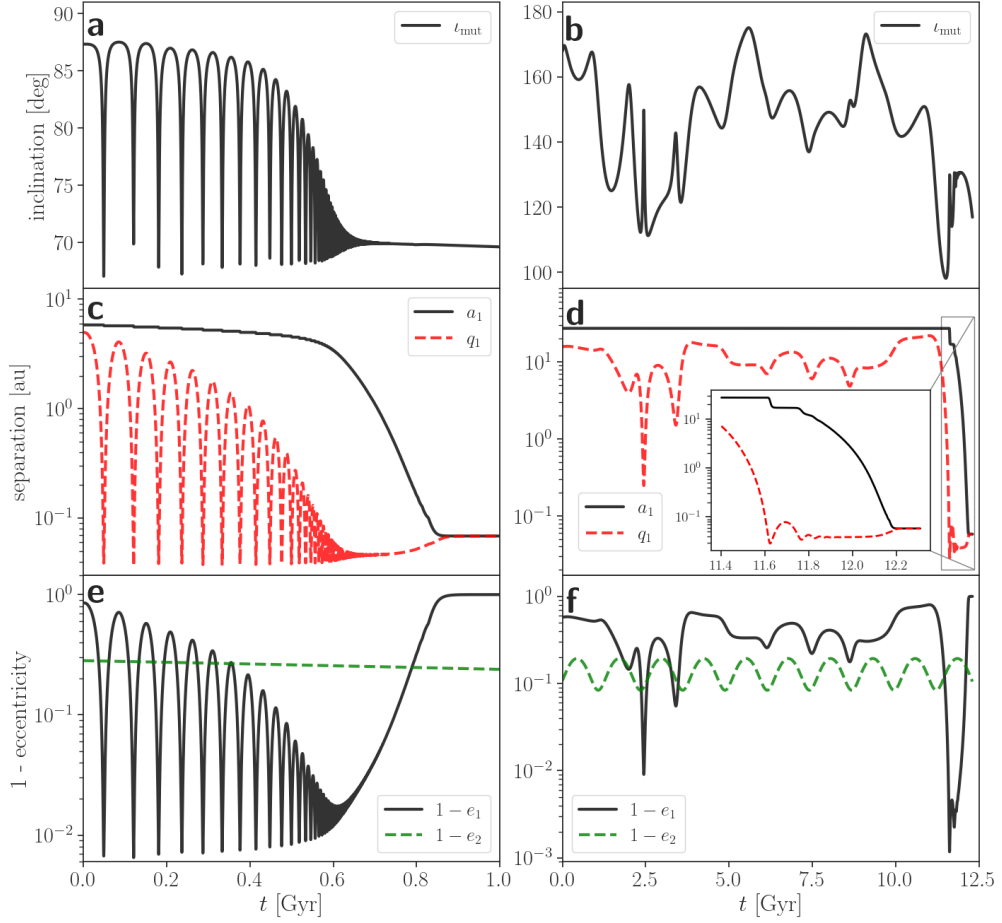


Fig. 2 Time evolution for regular and chaotic HJ formation pathways. Top: time evolution of the mutual inclination of a regular orbit (a) and a chaotic orbit (b). Middle: Evolution of the proto-HJ's semi-major axis and pericentre for a regular orbit (c) and a chaotic orbit (d). Bottom: Evolution of the inner (black) and outer (green) eccentricity of a regular orbit (e) and a chaotic orbit (f). The initial conditions for the regular orbit are $a_1 = 5.82$ au, $a_2 = 1522.07$ au, $e_1 = 0.15$, $e_2 = 0.72$, $i_1 \approx 45.9^\circ$, $i_2 \approx 103.2^\circ$, $\iota_{\text{mut}} \approx 87.3^\circ$, $\omega_1 \approx 59.7^\circ$, $\omega_2 \approx 118.6^\circ$, $\Omega_1 \approx 45.7^\circ$, $\Omega_2 \approx 118.5^\circ$, $m_1 = 1.15 M_\odot$, and $m_3 = 0.50 M_\odot$. The initial conditions for the chaotic orbit are $a_1 = 27.40$ au, $a_2 = 14540.34$ au, $e_1 = 0.42$, $e_2 = 0.89$; inclinations $i_1 \approx 138.3^\circ$, $i_2 \approx 30.2^\circ$, $\iota_{\text{mut}} \approx 167.9^\circ$, $\omega_1 \approx 261.7^\circ$, $\omega_2 \approx 192.4^\circ$, $\Omega_1 \approx 18.7^\circ$, $\Omega_2 \approx 337.7^\circ$, $m_1 = 0.66 M_\odot$, $m_3 = 0.65 M_\odot$.

are uniformly distributed in $\cos \iota_{\text{mut}}$. Additional initial conditions and the rationale for this sampling are detailed in the methods section. Each system was evolved until reaching either 13.5 Gyr or the main-sequence lifetime of the more massive star, approximated as $10 (m/M_\odot)^{-2.5}$ Gyr. The planet is considered disrupted if its pericentre, $q_1 = a_1(1 - e_1)$, falls below $2.7 a_{\text{Roche}}$ [30], with the Roche limit calculated

Galactic Tides	Disrupted	Hot Jupiters	Unstable
On	442^{+21}_{-21}	428^{+21}_{-21}	998^{+32}_{-32}
Off	388^{+20}_{-20}	239^{+15}_{-15}	0

Table 1 Outcome statistics with and without Galactic Tides. We classify systems as *disrupted* if they reach low pericentres (q_1), as *Hot Jupiters* if they reach low semi-major axes (a_1) and eccentricities e_1 , and *unstable* if the stability criterion in [29] is violated. The $1 - \sigma$ errors are from shot noise.

as $a_{\text{Roche}} = R_J(M_*/M_J)^{1/3}$. Successful HJ formation at time t is classified by a sufficiently circular orbit, $e_1(t) \leq 0.01$, and a loss of at least 90% of its initial orbital separation, $a_1(t) \leq 0.1a_1(0)$. Finally, systems can also become dynamically unstable [29] as the outer binary evolves due to GT over Gyr timescales.

Table 1 summarises the statistics of each outcome. Both cases yield comparable fractions of $442/5000 = 8.9\%$ and $388/5000 = 7.8\%$ disruptions, when including and excluding GT, respectively. The GT case produces significantly more successful HJ formation at $(428 \pm 21)/5000 = 8.56 \pm 0.42\%$, as compared to $(239 \pm 15)/5000 = 4.8 \pm 0.3\%$ when GT are not present. This represents an enhancing factor of $\approx 1.8 \pm 0.14$, indicating that GT predominantly boost secular excitation that drives tidal migration, rather than directly increasing disruption rates. Moreover, the GT case shows that $20 \pm 0.64\%$ of systems become unstable due to changes in the orbit of the wide binary—most likely resulting in planetary ejection that could account for $\sim 20\%$ of known free-floating Jovian planets [11]. In contrast, systems cannot become unstable and form free floating planets without GT, as the outer orbit remains dynamically unperturbed.

Panel (a) of Figure 3 shows the distribution of disrupted (squares) and migrated (circles) orbits in the $\mathcal{R}_0 - \iota_{\text{mut}}$ parameter space. Systems marked with stars correspond to those used in Figure 2. The migrated population exhibits a clear dichotomy: for systems with low $\cos \iota_{\text{mut}}$, standard ZLK migration operates on relatively short timescales $\lesssim 1$ Gyr, yielding extremely small values of \mathcal{R}_0 . This also includes systems with moderate $\cos \iota_{\text{mut}}$ and low \mathcal{R}_0 , which are driven by the octupole (eccentric) ZKL [20] (see methods). Once \mathcal{R}_0 exceeds a certain threshold, the initial mutual inclination becomes unconstrained and long-term chaotic evolution over $\gtrsim 1$ Gyr dominates. In contrast, disrupted orbits cluster at lower \mathcal{R}_0 values and occur predominantly at small $\cos \iota_{\text{mut}}$.

Panels (b) and (c) of Figure 3 show $a_1 - a_2$ correlations, coloured by $|\cos \iota_{\text{mut}}|$. In both simulations, disruptions occur mainly at low a_2 , where the short secular ZLK timescale ($t_{\text{sec}} \propto a_2^3$) prevents tides from damping eccentricity before disruption. HJ migration is favoured at larger a_2 when $a_1 \lesssim 100a_2$, while larger ratios tend to the disruption of HJs. In the GT case (b), an excess of HJs appear at $a_2 \gtrsim 10^4$ au and large $|\cos \iota_{\text{mut}}|$, also allowing initially coplanar systems to produce HJs. Without GT (c), wide-orbit HJ formation is sparse and $|\cos \iota_{\text{mut}}| \lesssim 0.6$ in most cases. These wide-binary HJs account for the difference seen in Table 1. Due to slow secular evolution, wide binaries rarely lead to the disruption of HJs, so the inclusion of GT does not significantly change disruption rates.

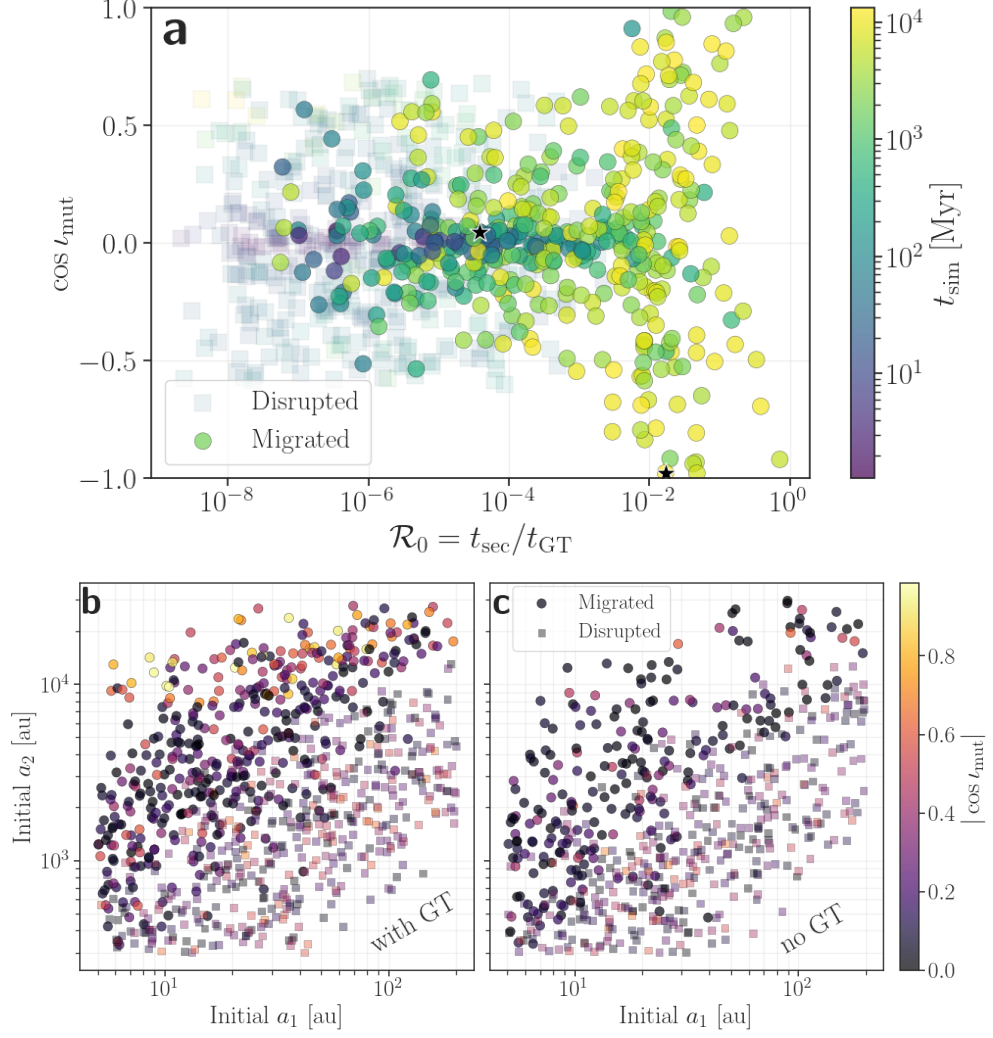


Fig. 3 Top panel: Initial $\cos i_{\text{mut}}$ versus \mathcal{R}_0 for the run with GT (a). Migrated (circles) and disrupted (squares) systems are color-coded by the total evolution time. Individual simulations in Figure 2 are also shown (stars). Bottom panels: a_1 - a_2 parameter space for the simulations with GT turned on (b) and off (c), coloured by the initial mutual inclination between the orbits ($|\cos i_{\text{mut}}|$).

Hot Jupiters around old stars

Figure 4 compares the delay-time distributions of planetary disruptions and HJ formation, with fits to observational data. Disruptions (red) typically occur much earlier than HJ formation in both models. When GT are included, 80% of disruptions occur within 1 Gyr, compared to 90% when GT are absent. In contrast, HJ formation is delayed: only 38% (55%) of HJs form within 1 Gyr with GT on (off). In the case without GT, our results align with previous findings: disruptions precede HJ mergers [7].

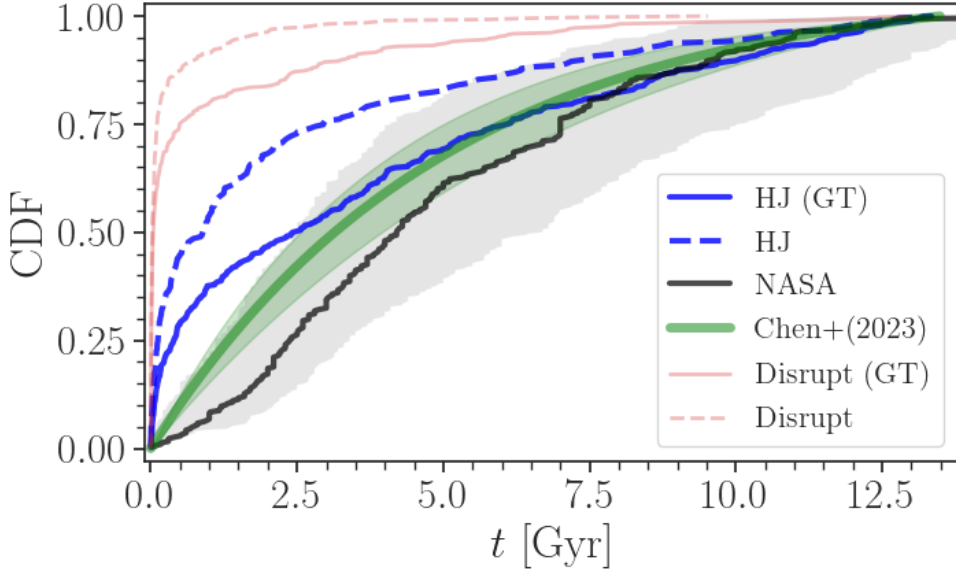


Fig. 4 Cumulative delay-time distributions of the simulations overlaid with stellar ages and fits. The occurrence rate fit in green is given by [10], while the HJ sample with known stellar ages from the *NASA exoplanet archive database* is in black, with measurement uncertainties represented by the gray shaded area. Disruptions are in red and HJ formation is in blue. Simulations with and without GT are represented by solid and dashed lines, respectively.

Notably, the GT model produces a significant fraction of very late-forming HJs—30% occur after 5 Gyr—whereas without GT this fraction drops to 17%.

To compare with observations, we performed a Table Access Protocol (TAP) search of the public NASA Exoplanet Archive database¹ for systems with known stellar ages and uncertainties, which returns 308 systems (see Methods). The resulting CDF is shown in black in Figure 4, with the gray shaded area indicating age uncertainties. For reference, we also plot the bias-corrected fitting formula from Chen et al. [10], where the probability distribution follows an exponential function as $f_{\text{HJ}} \propto \exp[-0.2 \pm 0.06(t/\text{Gyr})]$. This corresponds to the cumulative distribution function $\text{CDF}(\text{HJ}) \propto (1 - \exp[-0.2(t/\text{Gyr})])$. Its CDF and $1 - \sigma$ uncertainty are represented by the green line and shaded region, respectively. HJ formation times in simulations with GT are consistent with observed data for $t \gtrsim 2.5$ Gyr, encompassing 50% of cases. In contrast, without GT only $\sim 6\%$ of HJs fall within the green zone at ages $\gtrsim 9$ Gyr. Earlier HJ arrival is disfavoured due to the rapid tidal decay observed in many systems and the large stellar obliquities in older stars, both suggesting recent formation. Therefore, we conclude that the stellar age reflects the true formation age of HJs and that the wide-binary HJ-formation channel can reproduce most old HJs with stellar ages $\gtrsim 2.5$ Gyr.

¹<https://exoplanetarchive.ipac.caltech.edu/TAP-sync>

Broader Implications on Planets around Wide-Binary Systems

The total occurrence rate can be expressed as $\mathcal{R}_{\text{HJ}} = f_{\text{HJ}} f_{\text{bin}}^{\text{wide}} f_{\text{GP}}$, where $f_{\text{HJ}} \approx 8.6\%$ is the successful HJ formation fraction. The fraction of wide-binary systems $f_{\text{bin}}^{\text{wide}}$ is the product of the HJ-hosting total binary fraction of 50% and the fraction of wide binaries. The tightest binary systems that host Jovian planets have $a_2 \sim 20$ au [31], thus we estimate the wide fraction as $\log_{10}(3 \times 10^4 / 300) / \log_{10}(3 \times 10^4 / 20) \approx 0.63$, yielding $f_{\text{bin}}^{\text{wide}} \approx 31\%$. $f_{\text{GP}} \approx 10\text{--}15\%$ is the giant planet host fraction. Overall we get $\mathcal{R}_{\text{HJ}} \approx 26\text{--}40\%$ of the observed maximal $\sim 1\%$ occurrence rate. Without GT, this estimate drops to 14 – 22%, which is consistent with previous models (e.g. [21, 32]).

The occurrence rate was derived under conservative assumptions of the high end of the observed rate of 1%, which is compatible with the radial velocity (RV) samples. Transiting surveys such as Kepler find smaller occurrence rates of about 0.5%. This discrepancy rises due to the exclusion of spectroscopic binaries from the RV sample, while the Kepler sample is not sensitive to binarity. Thus, RV samples indicate the occurrence rate of HJs around single stars while transit surveys indicate occurrence rates around all stars [33]. Since binarity often precludes planet formation, ref. [18] suggested that the occurrence rates from magnitude-limited surveys underestimate the true occurrence rate by a factor of ~ 2 . Wide-binaries of $a_2 \gtrsim 10^3$ au are unlikely to hinder planet formation, thus we take the 1% as a fiducial value. Moreover, the 50% binary fraction can be higher due to an unknown sample of wide white-dwarfs or ejected companions [3]. Similarly, both stars can have their own Jovian planets which will further increase the occurrence rates [32].

The Cold/Hot Jupiter ratio obtained from the simulations with and without GT is $\approx 7.3 \pm 0.36$ and $\approx 18.3 \pm 1.18$, respectively. For a rough estimate, the total Cold/Hot Jupiter ratio is 14.6 ± 0.72 , assuming a 50% Jupiter host binary fraction, consistent with the ratio constrained by observations. Without GT, the Cold/Hot Jupiter ratio is 37.6 ± 2.36 , overestimated by a factor of 2.5–3.7 and consistent with previous models [7, 21].

The rate of free-floating giant planets (FFGP) is $20\% \times 0.15 \times 0.5 \approx 1.5\%$. The observed FFGP rate per star is estimated by $dN/d\log_{10} M_p = 2.18_{-1.40}^{+0.52} \times (M_p/8M_{\oplus})^{-p}$, where $p = 0.96_{-0.27}^{+0.47}$ [11]. For Jupiter-mass planets, ejection in wide binaries accounts for approximately $24_{-15}^{+117}\%$ of the population. The efficiency of this ejection mechanism is not reduced for larger Jupiter masses, so it is expected to remain robust for masses above Jupiter's, potentially explaining the higher-mass tail of FFGP. Planet-planet scattering efficiently produces free-floating rocky planets, but faces challenges to eject the most massive FFGP [34].

Our study adopts well-established equilibrium tide models and spin pseudo-synchronisation prescriptions [35] with fixed apsidal motion constants, omitting explicit obliquity evolution. This is justified as spins rapidly synchronise and obliquity distributions remain broadly consistent with observations [7]. We have confirmed the robustness of our results through an additional 5000 simulations including dynamical tides for highly eccentric binaries (see Methods). We fix planetary radii in our models, noting that cold Jupiters tend to have a small spread in radii around R_J while HJ tend to be more inflated due to tidal heating and intense stellar irradiation, both caused by their close proximity to the host star (see methods). Petrovich (2015) also explored

inflated HJ radii and did not find significant changes in overall rates [21]. Our Galactic tide treatment captures the dominant vertical component. More detailed Galactic tidal models and the effects of occasional stellar encounters have been explored for wide binaries by Stegmann et al. (2024) via direct N-body simulations [36]. However, applying such simulations to our systems—where the inner orbital timescales are much shorter and need to be resolved over $\gtrsim 10$ Gyr—remains extremely challenging.

We have shown that including GT-effects on wide-binary orbits over \sim Gyr timescales enhances the HJ-formation rate by 1.8 ± 0.14 . This, in turn, can explain 26 – 40% of all HJ and about $\sim 25\%$ of free-floating giant planets (with large uncertainties). This is likely a lower limit since HJs around single stars could have lost the wide binary companion due to stellar evolution [3]. Moreover, our wide-binary HJ-formation channel successfully reproduces the delay-time distribution of HJs around old stars with $t_{\text{age}} \gtrsim 2.5$ Gyr which can only form recently, making it the dominant formation channel for such systems. Finally, the destabilising effects of an evolving wide-binary orbit and planetary ejection reproduce the observed Cold/Hot Jupiter ratio, whereas the standard high-eccentricity channel without GT overproduces this ratio by a factor of 2.5 – 3.7. Future studies of more detailed tidal evolution, Galactic potential, and planetary structure will refine the formation rates and properties. This wide-binary channel can explain not only FFGPs and HJs, but also ultra-short-period planets whose formation rate increases with stellar age [37].

Methods

Secular dynamics

von Ziepel-Lidov-Kozai oscillations

Consider an inner binary consisting of bodies m_1 and m_2 with semi-major axis a_1 and eccentricity e_1 , the outer binary consists of the centre of mass on the inner binary and the third body m_3 , with a_2 and e_2 . The mutual inclination between the orbital planes is ι_{mut} . ZLK oscillations are large-amplitude exchanges between the eccentricity and inclination of the inner orbit, driven by the torque of the outer perturber that occur on long, secular time [38]

$$t_{\text{sec}} = \frac{8(1 - e_2^2)^{3/2}}{15\pi} \frac{m_{\text{tot}}}{m_3} \frac{P_{\text{out}}^2}{P_{\text{in}}} = \frac{16}{15} \frac{m_1^{1/2}}{G^{1/2} m_3} \frac{a_2^3 (1 - e_2^2)^{3/2}}{a_1^{3/2}} \quad (3)$$

where G is the gravitational constant, $m_{\text{tot}} = m_1 + m_2 + m_3$ is the total mass and we assume that the planetary mass is small, $m_2 \ll m_1, m_3$.

After double averaging over both orbits and truncating at the leading quadrupole order $\propto (a_1/a_2)^2$ in the test-particle limit, these oscillations preserve the inner orbit's semi-major axis a_1 and the z-component of the inner angular momentum $j_z = \sqrt{1 - e_1^2} \cos \iota_{\text{mut}}$ and the problem is integrable. The maximal eccentricity depends mostly on the mutual inclination (for initial quasi-circular orbit, see review of Naoz

(2016) [16]).

$$e_{\max} = \sqrt{1 - \frac{5}{3} \cos^2 \iota_{\text{mut}}} \quad (4)$$

However, for weak hierarchies, the double averaging approximation breaks down [39–41], and the expression for e_{\max} can be corrected for expansion in the period ratio to first order [42–45] and second order [46, 47].

At octupole order, j_z is no longer conserved and the evolution is chaotic, and orbital flips and extreme eccentricity excitations can occur for a wider range of parameter space [20, 48, 49]. The octupole parameter that governes the dynamics is:

$$\epsilon_{\text{oct}} = \frac{a_1 e_2}{a_2 (1 - e_2^2)}, \quad (5)$$

and the corresponding octupole timescale is [ref. 38, Eq. 79]:

$$t_{\text{oct}} = \frac{256\sqrt{10}}{15\pi\sqrt{\epsilon_{\text{oct}}}} t_{\text{sec}} \approx 17 \frac{t_{\text{sec}}}{\epsilon_{\text{oct}}^{1/2}} \propto \frac{a_2^{7/2} (1 - e_2^2)^2}{a_1^2 e_2}. \quad (6)$$

Although the excitation to high eccentricity occurs more frequently, more planetary disruption is 3–7 times more likely than HJ formation, depending on initial conditions [7, 21].

Figure 5 illustrates the enhanced eccentricity excitations due to the octupole effects. Contrary to the standard (quadrupole) ZLK, The 'Kozai constant' $\sqrt{1 - e_1^2} \cos \iota_{\text{mut}}$ is no longer conserved and the pericentre of the inner binary is gradually descends, as expected analytically [50]². The inclination range in this regime is larger since extreme eccentricity can be obtained more gradually. The argument of pericentre also evolves more chaotically with alternating phases of libration and full circulation. The timescale is also longer and takes $\sim 20t_{\text{sec}}$ to get decoupled compared to the much faster evolution in the quadrupole ZLK case.

Galactic Tides

The tidal field of the Galactic disc can perturb the orbits of wide binaries. A sketch of the wide triple system in the galactic disc is dipicted in Figure 1 in the main text. To leading order, the vertical tide is given by the potential [26, 27]:

$$U(x, y, z) = -\frac{Gm_{\text{tot}}}{\sqrt{x^2 + y^2 + z^2}} + 2\pi G\rho_0 z^2, \quad (7)$$

where $\rho_0 = 0.185 M_{\odot} \text{ pc}^{-3}$ is the local density and x, y, z are Cartesian distances from the galactic centre and m_{tot} is the total mass of the binary. After orbit-averaging, the corresponding secular Hamiltonian is given by:

$$\mathcal{H}_{\text{GT}} = -\frac{Gm_{\text{tot}}}{2a_2} + \pi G\rho_0 a_2^2 \sin^2 \iota_{\text{out}} (1 - e_2^2 + 5e_2^2 \sin^2 \omega_2), \quad (8)$$

²From Eq. 26 in [50] we have $t_{\text{descent}} \approx \Upsilon \eta t_{\text{oct}}$. In our case, $t_{\text{oct}} \approx 174t_{\text{sec}}$, $\eta \approx \sqrt{2r_p/a_1}/7$ and $\Upsilon \approx 7$ (see their appendix B), so $t_{\text{descent}} \approx 0.074t_{\text{oct}} \approx 15t_{\text{sec}}$, consistent with the number of ZLK cycles required to reach 0.03 au.

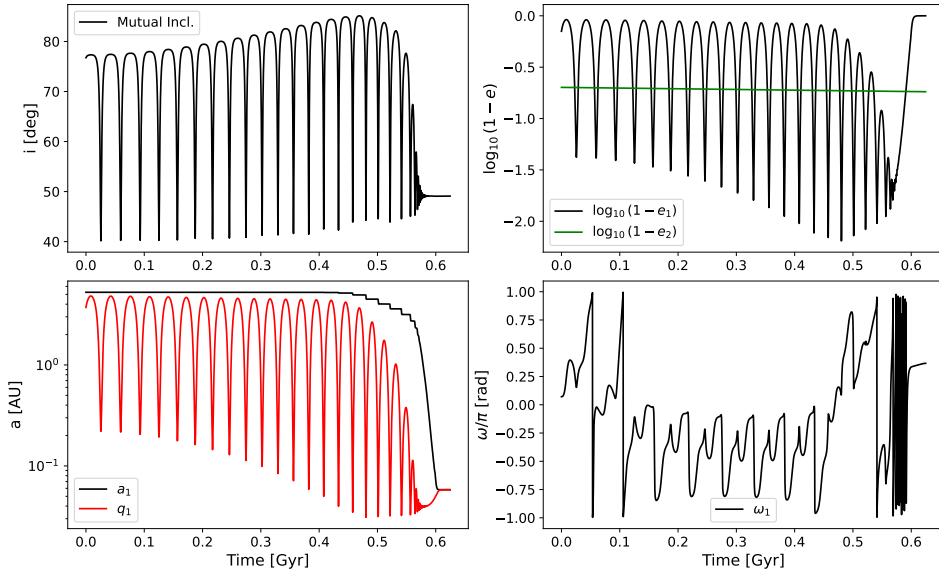


Fig. 5 Example of time evolution of a representative system which represents octupole-level ZLK dynamics. The initial conditions are: semi-major axes $a_1 = 5.25$ AU, $a_2 = 1236.74$ AU; eccentricities $e_1 = 0.29$, $e_2 = 0.80$; inclinations $i_1 \approx 48.1^\circ$, $i_2 \approx 107.3^\circ$, and mutual inclination $\iota_{\text{mut}} \approx 76.75^\circ$. The arguments of pericentre are $\omega_1 \approx 12.8^\circ$, $\omega_2 \approx 210.7^\circ$; and the longitudes of ascending node are $\Omega_1 \approx 117.5^\circ$, $\Omega_2 \approx 170.5^\circ$. The masses are $m_1 = 0.77 M_\odot$, $m_2 = M_J$, and $m_3 = 0.55 M_\odot$

where ι_{out} is the angle between the outer binary and the galactic plane, and ω_2 is the argument of pericentre of the outer orbit.

The secular evolution and phase space are morphologically similar to the ZLK structure [51]; the critical inclination for the onset of the oscillations is $\cos^2 \iota_c < 4/5$, or $\iota_c \approx 26.56^\circ$. For a given prograde inclination $\iota_{\text{out}} > \iota_c$ (with the equivalent reflection symmetry for retrograde inclinations), the maximal eccentricity is $e_{\text{max}} = (1 - (5/4) \cos^2 \iota_{\text{out}})^{1/2}$. Developing high eccentricity in wide binaries was first demonstrated by Heisler and Tremaine (1986) [26] in the context of Sun-grazing comets emanating from the Oort cloud.

The timescale for secular evolution driven by the Galactic tide is given by [26, 27] and provided in Equation 1 in the main text. The ratio \mathcal{R}_0 between the secular timescale and the GT timescale is given by Equation 2 in the main text. Chaotic evolution and extreme eccentricity is possible when the ZLK and galactic tide timescales are comparable ($\mathcal{R}_0 < 1$). For further details, discussion and astrophysical implications on the coupled evolution of wide stellar triples with galactic tides we refer to Grishin and Perets (2022) [27]. Here we focus on formation of HJs in wide binaries and use similar methods of population synthesis.

Population Synthesis

Numerical methods and code implementation

To study the role of chaotic dynamics in HJ formation via high-e migration in wide triple systems, we employ the secular evolution code SecuLab³ [27]. SecuLab solves the secular equations of motion for hierarchical triple systems up to octupole order, which uses the orbit-averaging principle and thus is faster than direct N-body codes. Additional corrections due to the Brown Hamiltonian [39, 40, 44] are also implemented. We use the eccentricity and normalised angular momentum vector elements \mathbf{e} , \mathbf{j} [e.g. 21, 52] for both orbits rather than the traditional Delaunay elements [see details and discussion in ref 49]. The external perturbation from the Galactic tide changes the invariable plane of the triple system, which causes inconsistencies in the Delaunay variables [48], while the vector elements are not sensitive to the choice of reference frame. We choose the reference frame to align with the Galactic plane. The equations of motion for the inner orbit are similar to the ones used in Petrovich (2015) [21], but without the spin vectors, which are assumed to be pseudo-synchronised. For the outer orbit, the equations of motion have both feedback from the inner orbit (although it is negligible for the test particle limit) and the effect from the Galactic tide Hamiltonian (Equation 8).

Beyond gravitational three-body interactions, SecuLab accounts for perturbations due to the Galactic tide on the outer orbit [27] and additional conservative and dissipative forces. The conservative forces include

i) General-Relativistic (GR) precession of the inner binary from the 1st post-Newtonian (PN) term.

ii) Apsidal precession due to tidal bulges on both the planet and star. The extra precession may limit the maximal eccentricity attained during the evolution [see details in 49]. Mangipudi et al. (2022) [43] derived analytical expressions for the maximal eccentricity including the 1PN term only, applicable for compact objects, while [53] extended the expression to include tidal bulges applicable for stars.

The dissipative forces include tidal friction [6, 35] and gravitational-wave emission, occurring at the 2.5PN order. In our case for fluid bodies, gravitational-wave emission is negligible compared to tidal dissipation. We use the equilibrium tide model [35]. We do not evolve the spin or the planet, but rather assume that the planetary spin is pseudo-synchronised with the orbit, which occurs much faster than tidal circularisation [35]. We discuss the implementation of dynamical tides and its effects on the results in later sections.

Initial conditions of the population study

In order to examine the role of the galactic tide in forming HJs, we run $N = 10^4$ dynamically stable systems according to Mardling and Aarseth (2001)'s stability criterion [29]. Mardling and Aarseth (2001)'s [29] criterion is applicable for triples of similar masses. Later studies updated the dependence with the mutual inclination and more extreme mass ratios [54–56], with initial conditions drawn as per Table 2. We run 1/2 of the simulation with GT and the other 1/2 without GT (so each run has

³Available at <https://github.com/evgenigrishin/SecuLab>

5,000 initial conditions). Table 2 lists our choices for the initial distribution of the parameters. We motivate our choices for the population study below:

Masses: The occurrence rate of HJs is dependent on the survey, its biases and completeness. The Kepler mission targeted primarily FGK stars, which are intrinsically brighter, easier to monitor with high photometric precision, and more amenable to RV follow-up than faint, active M dwarfs. RV surveys tend to find an increase of the occurrence rate with the star. However, recent analysis of TESS found that HJs are more common around lower mass GK stars which peak at around $0.8M_{\odot}$ [33, 57]. The occurrence rates around M dwarfs in the range of $0.45 - 0.65M_{\odot}$ is much lower, about $0.27 \pm 0.09\%$ [58]. This trend is, however, most likely determined by the metallicity [59], since HJ occur around more metal-rich stars [1] and more massive stars are more diverse in their metallicity. Having no definitive observed trend with the stellar mass, we remain agnostic to the initial mass distribution and simply sample the stellar masses from The Kroupa mass function ($m_1, m_3 \propto m^{-2.3}$) and use the mass radius power law $R \propto m^{\xi}$ with $\xi = 0.8$ for $m < M_{\odot}$ and $\xi = 0.57$ for $m > M_{\odot}$ [60]. The planetary masses and radii are kept at the Jovian values. The mass does not play a role in the dynamics since the system is always in the test particle limit. Also, the radius is almost independent of the mass (see more details and discussion in the mass-radius relation section).

Semi-major axes: For the wide stellar binaries the distribution of semi-major axes is consistent with earlier studies [61] and more recent data available from Gaia [62]. The spatial distribution of giant planets, especially beyond the snow ice at a few au, is less constrained. According to [8], the giant planet distribution peaks at $3.6^{+2.0}_{-1.8}$ au and afterwards decays as a power law $\propto a^{\beta}$ with $\beta = -0.86 \pm 0.41$, consistent with a log-uniform distribution ($\beta = -1$). The occurrence rate then decays for separations above 10 au, but suffers from completeness of the observed data. This present-day distribution may differ from the zero-age distribution. For simplicity, we choose a log-uniform distribution between $5 \leq a(\text{au}) \leq 200$.

Eccentricities: For wide binaries, recent analysis by Gaia shows that the eccentricity distribution is consistent with a thermal distribution [62]. Very wide binaries could have slightly superthermal distributions [63, 64], but we keep the initial eccentricity distribution as thermal for simplicity. The planetary eccentricity is sampled from a Rayleigh distribution with $\sigma = 0.2$, as motivated by Moorhead et al. [65], which studied the distribution of transit durations for Kepler planet candidates and their implications for orbital eccentricities. Similar initial Rayleigh eccentricity distribution indicates that the cold Jupiter population is consistent with high-e migration [4].

Inclinations and other angles: The mutual inclination between the planetary and the wide stellar orbit is uniform in cosine. In practice, each inclination ι_i is sampled with respect to the plane of the galaxy. The mutual inclination is given by the cosine theorem

$$\cos \iota_{\text{mut}} = \cos \iota_1 \cos \iota_2 + \sin \iota_1 \sin \iota_2 \cos(\Omega_1 - \Omega_2). \quad (9)$$

The result is also uniform in cosine, as seen in Figure 7 in [27]. This (cosine) uniform distribution is motivated by the recent analysis of [66] where all planets in binaries of separations above 700 au have randomised angles. In fact, only the smaller planets ($R < 6R_{\oplus}$) are aligned for binaries for separations below 700 au, and giant planets are

Parameter	Distribution / Value
m_1, m_3	Power law: $f(m) \propto m^{-2.3}$, $m \in [0.5, 1.5] M_\odot$
m_2	$M_J = 0.0009546 M_\odot$
r_1, r_3	Mass-radius relation
r_2	$R_J = 0.10276 R_\odot$
a_1	$\log U \sim [5, 200]$ au
a_2	$\log U \sim [300, 3 \times 10^4]$ au
e_1	Rayleigh: $f(e) = (e/\sigma^2) \exp(-e^2/2\sigma^2)$; $\sigma = 0.2$
e_2	Thermal: $f(e) = 2e$
ι_1, ι_2	$\cos \iota \sim U[-1, 1]$
ω_1, ω_2	$U[0, 2\pi]$
Ω_1, Ω_2	$U[0, 2\pi]$
k_*, k_p	0.028, 0.37
$t_{\nu*}, t_{\nu,p}$	50 yr, 0.01 yr

Table 2 Initial conditions for the simulations. Masses m_1 and m_3 are drawn from a power-law distribution with index -2.3 in the range $[0.5, 1.5] M_\odot$, while m_2 is fixed to one Jupiter mass. Radii r_1 and r_3 are calculated via a mass-radius relation, and r_2 is fixed to Jupiter's radius. semi-major axes a_1 and a_2 are drawn from log-uniform distributions. Eccentricity e_1 is sampled from a Rayleigh distribution with $\sigma = 0.2$, and e_2 from a thermal distribution. Angular parameters are uniformly sampled.

misaligned for any separation. The other angles (arguments of pericentre ω_i , argument of ascending node Ω_i) are sampled uniformly.

The **stopping conditions** are similar to [27]:

1. The system becomes dynamically unstable according to [29].
2. The planet reaches a pericentre small enough to be disrupted: $r_{\text{peri}} < 2.7a_{\text{Roche}}$, where $a_{\text{Roche}} = R_p(M_*/M_p)^{1/3}$, consistent with [30]'s hydrodynamical simulations for planetary disruption.
3. The eccentricity of the planet, e_1 , satisfies $e_1 \leq 0.01$, and the final semi-major axis is 10% smaller than the initial value.
4. The maximum simulation time of 13.5 Gyr or the main-sequence lifetime of the more massive star $t_{\text{ms}} = 10 m^{-5/2}$ Gyr has been reached, where $m = \max\{m_1, m_2\}/M_\odot$.

Exoplanet archive TAP search and data selection

We obtain publicly available exoplanet data from the Exoplanet archive database: <https://exoplanetarchive.ipac.caltech.edu/TAP-sync>. We only retrieve exoplanets with masses $0.3 M_J \leq M_p \leq 13 M_J$ for which the host star's age and planetary radii are known, and stellar masses are in the range $0.5 M_\odot < M_* \leq 1.5 M_\odot$. We use the following ADQL query:

We follow by further slicing the period to $P < 10$ days and $e < 0.1$, returning 308 planets as of 4 September 2025.

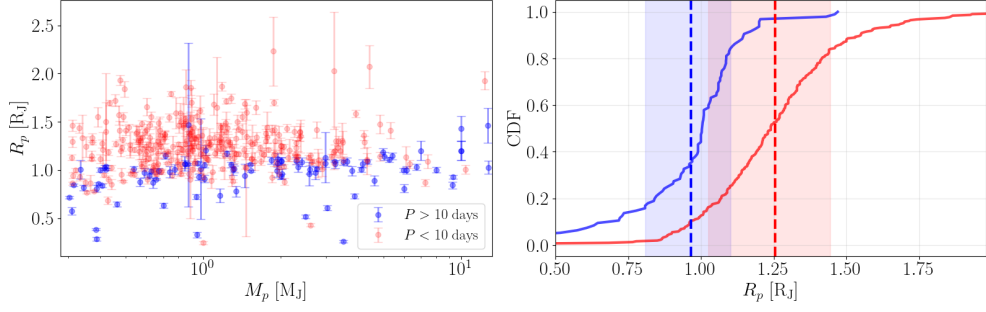


Fig. 6 Left: Mass-Radius distribution for HJ ($P < 10$ days, red) and cold/warm Jupiters ($P > 10$ days, blue). Right: CDFs of the data on the left panel. Dashed lines are the mean values and the shaded regions represent the $1 - \sigma$ confidence levels.

Listing 1 Table Access Protocol (TAP) search query

```
SELECT DISTINCT pl_name, pl_orbsmax, pl_bmassj, pl_orbeccen, pl_orbper,
    st_mass, st_age, st_ageerr1, st_ageerr2, pl_radj, pl_radjerr1, pl_radjerr2
FROM ps
WHERE pl_bmassj BETWEEN 0.3 AND 13
    AND st_mass BETWEEN 0.5 AND 1.5
    AND pl_orbsmax IS NOT NULL
    AND st_age IS NOT NULL
    AND st_ageerr1 IS NOT NULL
    AND pl_radj IS NOT NULL
    AND pl_radjerr1 IS NOT NULL
```

Giant Planet Mass-Radius Relation

Bashi et al. (2017) [67] found the mass-radius relationship for giant planets $R \propto M^{0.01 \pm 0.02}$. Recently updated, Müller et al. (2024) [68] found $R \propto M^{-0.06 \pm 0.07}$, both consistent with flat ratios. Already formed HJs are highly-irradiated by the host star, so their radii may be inflated [69]. Young Jupiters, in contrast, may still be thermally contracting. This will affect their coupled tidal evolution as it is a strong function of the planetary radius [70, 71]. However, since the typical HJ-formation timescales are of the order of Gyr, we fix the radius at $1R_J$ for simplicity and do not attempt to adjust for the post HJ-formation inflation, which is beyond the scope of this work. We finish this section by comparing the sample of HJ with the cold Jupiter sample that consists of 95 planets with known stellar ages and planetary radii. Cold Jupiters are usually discovered via radial velocities where radii are unknown, so this sample is far from complete.

The left panel of Figure 6 shows the mass-radius relationship for HJs ($P < 10$ days and $e < 0.1$, red) and Cold/Warm Jupiters ($P > 10$ days, blue). It is worth noting that Cold Jupiters have radii close to $\sim 1R_J$ and, as expected, they are independent of the mass [67, 68]. On the contrary, the HJ sample has a much larger mean radius. This is also evident from the right-hand panel, which shows the CDF for both populations.

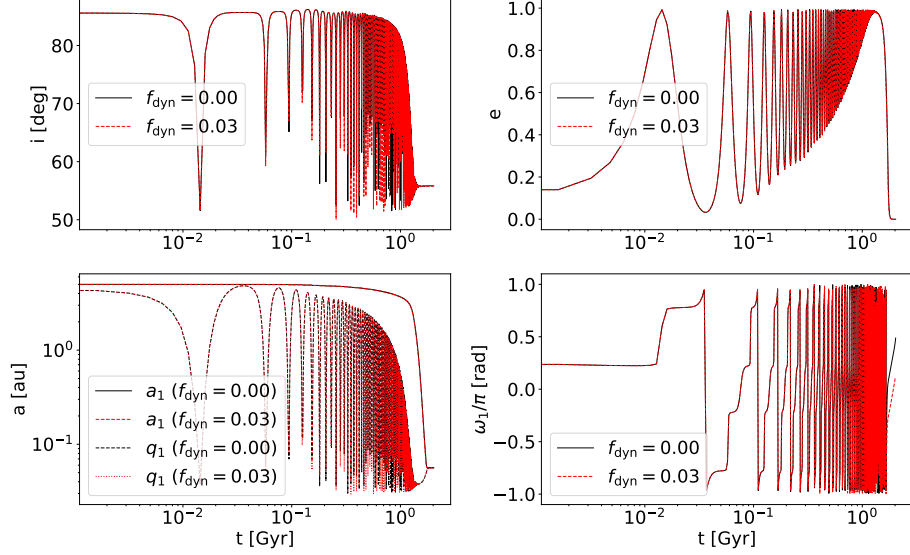


Fig. 7 Comparison of orbital evolution for a HD 80606b-like system with different dynamical friction parameters, $f_{\text{dyn}} = 0.00$ (black solid lines) and $f_{\text{dyn}} = 0.03$ (red dashed lines). The plots show inclination (i), eccentricity (e), semi-major axis (a_1 and pericenter q_1), and argument of periapsis (ω_1/π) as functions of time. The close agreement indicates that moderate changes in f_{dyn} do not significantly affect the orbital evolution over the timescales of our simulations.

In this panel, dashed lines are mean values and the shaded regions represent the $1 - \sigma$ confidence levels. The Cold and Hot Jupiter populations have $R_{\text{CJ}} = 0.96^{+0.14}_{-0.16} R_{\text{J}}$ and $R_{\text{HJ}} = 1.25^{+0.19}_{-0.23} R_{\text{J}}$, respectively.

The stellar ages and uncertainties of the 308 HJ systems were previously analysed and plotted in Figure 4.

Dynamical tides in eccentric binaries

We have used a simplified model for equilibrium tides based on a fixed value of the apsidal motion constants and the viscous times [35]. The apsidal motion constants $k_p = 0.37$ and $k_{\star} = 0.028$ were taken from ref. [7]. For the viscous time we use $t_{\nu,\star} = 50$ yr and $t_{\nu,p} = 0.01$ yr, following ref. [4] which follows ref.[21].

We also implement a model for dynamical tides in highly eccentric binaries following refs. [27, 72]. In particular, we follow Grishin and Perets (2022) [27] and keep both tidal prescriptions. There will be an effective eccentricity e_{eff} where the equilibrium tide will dominate below $e < e_{\text{eff}}$ [see Sec. 2.4.3 in 27]. This is contrary to a switch at $e = 0.8$ implemented in [72] that makes the tidal prescription discontinuous. In particular, the energy loss during the pericentre passage due to dynamical tides raised on body 2 (the planet) by body 1 (the star) is

$$\Delta E_{1 \rightarrow 2} = f_{\text{dyn}} \frac{m_1 + m_2}{m_1} \frac{G m_2^2}{R_1} \left(\frac{R_1}{a_1(1 - e_1)} \right)^9, \quad (10)$$

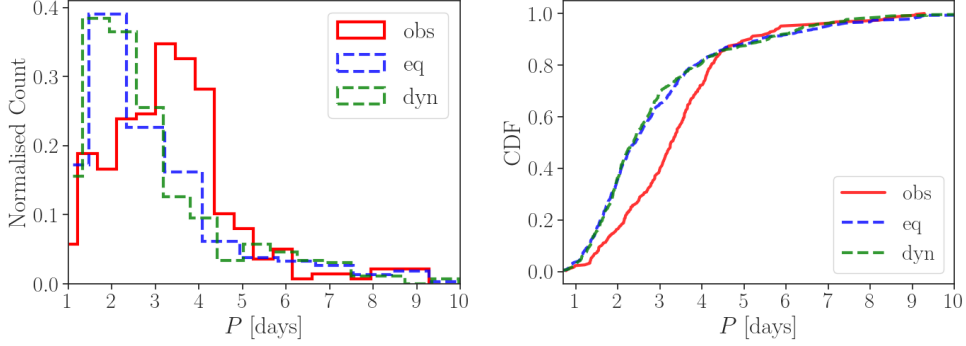


Fig. 8 Left: normalised histogram of the period distribution of the observed sample (solid red lines), the simulated models with equilibrium (blue) and dynamical (green) tides before reweighting (dotted lines) and after reweighting (dashed lines). Right: The same data but for the cumulative distribution function (CDF).

with a similar expression for $\Delta E_{2 \rightarrow 1}$ (keeping the pericentre term $a_1(1 - e_1)$ unchanged). The efficiency of the dynamical tide is encapsulated in f_{dyn} . We ran an additional set of 5000 simulations with $f_{\text{dyn}} = 0.03$ and did not find significant changes for the population analysis. We obtained 426 HJs, 450 disruptions, and 964 unstable giant planets, which is consistent with the run without including dynamical tides. These results are also supported by previous findings, showing that the efficiency of tidal migration is essentially independent on the tidal model selected [21, 73]. For a quantitative test case, we have reproduced the evolution of HD 80606 b with and without dynamical tides, using the same initial conditions and tidal parameters as in ref. [17]. We did not find any significant difference in the evolution as shown in Figure 7.

Nevertheless, more detailed modelling of dynamical and chaotic tides will be necessary. The dominant f -mode energy can random-walk to large values and could be efficient in extracting orbital energy from very eccentric objects near their Roche limit [e.g., 74–76]. The resulting model could prevent some HJs from undergoing tidal disruption. While [77] argues that most proto-HJs could avoid tidal disruption and efficiently decouple from the wider binary, the population study by [78] found a modest increase in the HJ formation rate, explaining at most 20 – 30% of HJs. If indeed tidal dissipation is efficient, this could explain most HJs along with the inclusion of GT on wide binaries. However, efficient tidal evolution may also skew the delay-time distribution so that HJs will form after a few ZLK cycles. This would pose a challenge to the late-forming HJs such as NGTS-10b [9], or TOI-2019b which is found around a star with $t_{\text{age}} = 1.77^{+0.88}_{-0.68}$ Gyr and is expected to disrupt in a few Myr [79].

Period Distribution

We compare the observed period distribution of HJs with the results from our simulations. As seen in the histogram on the left panel of Figure 8, the simulated HJs (for both equilibrium and dynamical tide modes) have shorter periods than the observed

ones. The right panel of Figure 8 shows the CDF of the same data. Although the simulated data has indeed more short period orbits, the HJ population with orbits longer than ~ 4.5 days is compatible with the simulated data.

The discrepancy may be explained by several effects: As discussed in the initial condition for the population study, the observed masses are different from the sampled masses and suffer from observational biases. The masses affect the period distributions via the strength of the tidal dissipation and setting the Roche limit for a disruption event in lieu of a HJ formation.

Additional effects we have not included are dynamical tides in the form of inertial waves in convective envelopes and internal gravity waves in stellar radiative regions, which operate even for circular and spin-synchronised HJ systems. These effects induce a fast tidal disruption for some of the simulated HJs, as observed in TOI 2019b and NGTS-10 [9, 79], which will eliminate HJs on short period orbits that formed too early from the observed sample. A self-consistent analysis that consists of eccentric tidal migration, subsequent tidal evolution and hierarchical Bayesian modelling that estimates the observability of the simulated data, its implications, and comparison to the observed stellar age and orbital distribution is planned for future work (Alvarado-Montes, Grishin et al., 2025, in prep.).

Acknowledgements

We thank Sharan Banagiri, Alexey Bobrick, Ryosuke Hirai and Hagai B. Perets for useful discussions. EG acknowledges support from the ARC Discovery Program DP240103174 (PI: Heger). JAAM acknowledges support from the Macquarie University Research Fellowship (MQRF) scheme.

Declarations

The authors declare no conflict of interest.

References

- [1] Johnson, J.A., Aller, K.M., Howard, A.W., Crepp, J.R.: Giant Planet Occurrence in the Stellar Mass-Metallicity Plane. *Publ. Astron. Soc. Pac.* **122**(894), 905 (2010) <https://doi.org/10.1086/655775> [arXiv:1005.3084](https://arxiv.org/abs/1005.3084) [astro-ph.EP]
- [2] Dawson, R.I., Johnson, J.A.: Origins of Hot Jupiters. *Annu. Rev. Astron. Astrophys.* **56**, 175–221 (2018) <https://doi.org/10.1146/annurev-astro-081817-051853> [arXiv:1801.06117](https://arxiv.org/abs/1801.06117) [astro-ph.EP]
- [3] Stephan, A.P., Martin, D.V., Naoz, S., Hughes, N.R., Shariat, C.: Two Novel Hot Jupiter Formation Pathways: How White Dwarf Kicks Shape the Hot Jupiter Population. *Astrophys. J. Lett.* **977**(1), 11 (2024) <https://doi.org/10.3847/2041-8213/ad94d8> [arXiv:2408.13307](https://arxiv.org/abs/2408.13307) [astro-ph.EP]

[4] Weldon, G.C., Naoz, S., Hansen, B.M.S.: The Cold Jupiter Eccentricity Distribution is Consistent with EKL Driven by Stellar Companions. *Astrophys. J. Lett.* **980**(2), 31 (2025) <https://doi.org/10.3847/2041-8213/adb157> arXiv:2411.05066 [astro-ph.EP]

[5] Albrecht, S.H., Dawson, R.I., Winn, J.N.: Stellar Obliquities in Exoplanetary Systems. *Publ. Astron. Soc. Pac.* **134**(1038), 082001 (2022) <https://doi.org/10.1088/1538-3873/ac6c09> arXiv:2203.05460 [astro-ph.EP]

[6] Fabrycky, D., Tremaine, S.: Shrinking Binary and Planetary Orbits by Kozai Cycles with Tidal Friction. *Astrophys. J.* **669**(2), 1298–1315 (2007) <https://doi.org/10.1086/521702> arXiv:0705.4285 [astro-ph]

[7] Anderson, K.R., Storch, N.I., Lai, D.: Formation and stellar spin-orbit misalignment of hot Jupiters from Lidov-Kozai oscillations in stellar binaries. *Mon. Not. R. Astron. Soc.* **456**(4), 3671–3701 (2016) <https://doi.org/10.1093/mnras/stv2906> arXiv:1510.08918 [astro-ph.EP]

[8] Fulton, B.J., Rosenthal, L.J., Hirsch, L.A., Isaacson, H., Howard, A.W., Dedrick, C.M., Sherstyuk, I.A., Blunt, S.C., Petigura, E.A., Knutson, H.A., Behmard, A., Chontos, A., Crepp, J.R., Crossfield, I.J.M., Dalba, P.A., Fischer, D.A., Henry, G.W., Kane, S.R., Kosiarek, M., Marcy, G.W., Rubenzahl, R.A., Weiss, L.M., Wright, J.T.: California Legacy Survey. II. Occurrence of Giant Planets beyond the Ice Line. *Astrophys. J. Suppl. Ser.* **255**(1), 14 (2021) <https://doi.org/10.3847/1538-4365/abfcc1> arXiv:2105.11584 [astro-ph.EP]

[9] McCormac, J., Gillen, E., Jackman, J.A.G., Brown, D.J.A., Bayliss, D., Wheatley, P.J., Anderson, D.R., Armstrong, D.J., Bouchy, F., Briegal, J.T., Burleigh, M.R., Cabrera, J., Casewell, S.L., Chaushev, A., Chazelas, B., Chote, P., Cooke, B.F., Costes, J.C., Csizmadia, S., Eigmüller, P., Erikson, A., Foxell, E., Gänsicke, B.T., Goad, M.R., Günther, M.N., Hodgkin, S.T., Hooton, M.J., Jenkins, J.S., Lambert, G., Lendl, M., Longstaff, E., Louden, T., Moyano, M., Nielsen, L.D., Pollacco, D., Queloz, D., Rauer, H., Raynard, L., Smith, A.M.S., Smalley, B., Soto, M., Turner, O., Udry, S., Vines, J.I., Walker, S.R., Watson, C.A., West, R.G.: NGTS-10b: the shortest period hot Jupiter yet discovered. *Mon. Not. R. Astron. Soc.* **493**(1), 126–140 (2020) <https://doi.org/10.1093/mnras/staa115> arXiv:1909.12424 [astro-ph.EP]

[10] Chen, D.-C., Xie, J.-W., Zhou, J.-L., Dong, S., Yang, J.-Y., Zhu, W., Liu, C., Huang, Y., Xiang, M.-S., Wang, H.-F., Zheng, Z., Luo, A.-L., Zhang, J.-H., Zhu, Z.: The evolution of hot Jupiters revealed by the age distribution of their host stars. *Proceedings of the National Academy of Science* **120**(45), 2304179120 (2023) <https://doi.org/10.1073/pnas.2304179120> arXiv:2311.00305 [astro-ph.EP]

[11] Sumi, T., Koshimoto, N., Bennett, D.P., Rattenbury, N.J., Abe, F., Barry, R., Bhattacharya, A., Bond, I.A., Fujii, H., Fukui, A., Hamada, R., Hirao, Y., Silva, S.I., Itow, Y., Kirikawa, R., Kondo, I., Matsubara, Y., Miyazaki, S., Muraki, Y.,

Olmschenk, G., Ranc, C., Satoh, Y., Suzuki, D., Tomoyoshi, M., Tristram, P.J., Vandorou, A., Yama, H., Yamashita, K.: Free-floating Planet Mass Function from MOA-II 9 yr Survey toward the Galactic Bulge. *Astron. J.* **166**(3), 108 (2023) <https://doi.org/10.3847/1538-3881/ace688> arXiv:2303.08280 [astro-ph.EP]

[12] Mayor, M., Queloz, D.: A Jupiter-mass companion to a solar-type star. *Nature* **378**(6555), 355–359 (1995) <https://doi.org/10.1038/378355a0>

[13] Yee, S.W., Winn, J.N., Hartman, J.D., Rodriguez, J.E., Zhou, G., Latham, D.W., Quinn, S.N., Bieryla, A., Collins, K.A., Eastman, J.D., Collins, K.I., Conti, D.M., Jensen, E.L.N., Anderson, D.R., Baştürk, Ö., Baker, D., Barkaoui, K., Battle, M.P., Bayliss, D., Beatty, T.G., Beletsky, Y., Belinski, A.A., Benkhaldoun, Z., Benni, P., Bosch-Cabot, P., Briceño, C., Brudny, A., Burleigh, M.R., Butler, R.P., Chairetas, S., Chontos, A., Christiansen, J., Ciardi, D.R., Clark, C.A., Cloutier, R., Craig, M.W., Crane, J.D., Dowling, N., Dressing, C.D., Emmanuel, J., Evans, P., Everett, M.E., Fernández-Rodríguez, G., Fernández Fernández, J., Forés-Toribio, R., Fortenbach, C.D., Fukui, A., Furlan, E., Gan, T., Ghachoui, M., Giacalone, S., Gill, S., Gillon, M., Hall, K., Hayashi, Y., Hedges, C., Higuera, J., Hintz, E.G., Hirsch, L., Holcomb, R., Horne, K., Grau Horta, F., Howard, A.W., Howell, S.B., Isaacson, H., Jenkins, J.M., Kagetani, T., Kamler, J., Kendall, A., Korth, J., Kroft, M.A., Lacedelli, G., Laloum, D., Law, N., Pitogo de Leon, J., Levine, A.M., Lewin, P., Logsdon, S.E., Lund, M.B., Madsen, M.M., Mann, A.W., Mann, C.R., Maslenikova, N.A., Matutano, S., McCormack, M., McLeod, K.K., Michaels, E.J., Mireles, I., Mori, M., Muñoz, J.A., Murgas, F., Narita, N., O'Brien, S.M., Odden, C., Palle, E., Patel, Y.G., Plavchan, P., Polanski, A.S., Popowicz, A., Radford, D.J., Reed, P.A., Relles, H.M., Rice, M., Ricker, G.R., Safonov, B.S., Savel, A.B., Schulte, J., Schwarz, R.P., Schweiker, H., Seager, S., Sefako, R., Shectman, S.A., Shporer, A., Stephens, D.C., Stockdale, C., Striegel, S., Tan, T.-G., Teske, J.K., Timmermans, M., Ulmer-Moll, S., Wang, G., Wheatley, P.J., Yalcinkaya, S., Zambelli, R., Van Zandt, J., Ziegler, C.: The TESS Grand Unified Hot Jupiter Survey. III. Thirty More Giant Planets. arXiv e-prints, 2507-01855 (2025) <https://doi.org/10.48550/arXiv.2507.01855> arXiv:2507.01855 [astro-ph.EP]

[14] Knudstrup, E., Albrecht, S.H., Winn, J.N., Gandolfi, D., Zanazzi, J.J., Person, C.M., Fridlund, M., Marcussen, M.L., Chontos, A., Keniger, M.A.F., Eisner, N.L., Bieryla, A., Isaacson, H., Howard, A.W., Hirsch, L.A., Murgas, F., Narita, N., Palle, E., Kawai, Y., Baker, D.: Obliquities of exoplanet host stars: Nineteen new and updated measurements, and trends in the sample of 205 measurements. *Astron. Astrophys.* **690**, 379 (2024) <https://doi.org/10.1051/0004-6361/202450627> arXiv:2408.09793 [astro-ph.EP]

[15] Chatterjee, S., Ford, E.B., Matsumura, S., Rasio, F.A.: Dynamical Outcomes of Planet-Planet Scattering. *Astrophys. J.* **686**(1), 580–602 (2008) <https://doi.org/10.1086/590227> arXiv:astro-ph/0703166 [astro-ph]

- [16] Naoz, S.: The Eccentric Kozai-Lidov Effect and Its Applications. *Annu. Rev. Astron. Astrophys.* **54**, 441–489 (2016) <https://doi.org/10.1146/annurev-astro-081915-023315> arXiv:1601.07175 [astro-ph.EP]
- [17] Wu, Y., Murray, N.: Planet Migration and Binary Companions: The Case of HD 80606b. *Astrophys. J.* **589**(1), 605–614 (2003) <https://doi.org/10.1086/374598> arXiv:astro-ph/0303010 [astro-ph]
- [18] Moe, M., Kratter, K.M.: Impact of binary stars on planet statistics - I. Planet occurrence rates and trends with stellar mass. *Mon. Not. R. Astron. Soc.* **507**(3), 3593–3611 (2021) <https://doi.org/10.1093/mnras/stab2328> arXiv:1912.01699 [astro-ph.EP]
- [19] Offner, S.S.R., Moe, M., Kratter, K.M., Sadavoy, S.I., Jensen, E.L.N., Tobin, J.J.: The Origin and Evolution of Multiple Star Systems. In: Inutsuka, S., Aikawa, Y., Muto, T., Tomida, K., Tamura, M. (eds.) *Protostars and Planets VII*. Astronomical Society of the Pacific Conference Series, vol. 534, p. 275 (2023). <https://doi.org/10.48550/arXiv.2203.10066>
- [20] Naoz, S., Farr, W.M., Rasio, F.A.: On the Formation of Hot Jupiters in Stellar Binaries. *Astrophys. J. Lett.* **754**(2), 36 (2012) <https://doi.org/10.1088/2041-8205/754/2/L36> arXiv:1206.3529 [astro-ph.EP]
- [21] Petrovich, C.: Steady-state Planet Migration by the Kozai-Lidov Mechanism in Stellar Binaries. *Astrophys. J.* **799**(1), 27 (2015) <https://doi.org/10.1088/0004-637X/799/1/27> arXiv:1405.0280 [astro-ph.EP]
- [22] Kunimoto, M., Matthews, J.M.: Searching the Entirety of Kepler Data. II. Occurrence Rate Estimates for FGK Stars. *Astron. J.* **159**(6), 248 (2020) <https://doi.org/10.3847/1538-3881/ab88b0> arXiv:2004.05296 [astro-ph.EP]
- [23] Alvarado-Montes, J.A., Sucerquia, M., García-Carmona, C., Zuluaga, J.I., Spitler, L., Schwab, C.: The impact of tidal friction evolution on the orbital decay of ultra-short-period planets. *Mon. Not. R. Astron. Soc.* **506**(2), 2247–2259 (2021) <https://doi.org/10.1093/mnras/stab1081> arXiv:2104.05967 [astro-ph.EP]
- [24] Li, J., Rix, H.-W., Ting, Y.-S., Müller-Horn, J., El-Badry, K., Liu, C., Seeburger, R., Green, G.M., Zhang, X.: Millions of Main-Sequence Binary Stars from Gaia BP/RP Spectra. arXiv e-prints, 2507-09622 (2025) <https://doi.org/10.48550/arXiv.2507.09622> arXiv:2507.09622 [astro-ph.SR]
- [25] Shariat, C., El-Badry, K., Naoz, S.: 10,000 Resolved Triples from Gaia: Empirical Constraints on Triple Star Populations. arXiv e-prints, 2506-16513 (2025) <https://doi.org/10.48550/arXiv.2506.16513> arXiv:2506.16513 [astro-ph.SR]
- [26] Heisler, J., Tremaine, S.: The influence of the Galactic tidal field on the Oort comet cloud. *Icarus* **65**(1), 13–26 (1986) [https://doi.org/10.1016/0019-1035\(86\)](https://doi.org/10.1016/0019-1035(86))

- [27] Grishin, E., Perets, H.B.: Chaotic dynamics of wide triples induced by galactic tides: a novel channel for producing compact binaries, mergers, and collisions. *Mon. Not. R. Astron. Soc.* **512**(4), 4993–5009 (2022) <https://doi.org/10.1093/mnras/stac706> [arXiv:2112.11475](https://arxiv.org/abs/2112.11475) [astro-ph.SR]
- [28] Grishin, E., Lai, D., Perets, H.B.: Chaotic quadruple secular evolution and the production of misaligned exomoons and Warm Jupiters in stellar multiples. *Mon. Not. R. Astron. Soc.* **474**(3), 3547–3556 (2018) <https://doi.org/10.1093/mnras/stx3005> [arXiv:1710.05920](https://arxiv.org/abs/1710.05920) [astro-ph.EP]
- [29] Mardling, R.A., Aarseth, S.J.: Tidal interactions in star cluster simulations. *Mon. Not. R. Astron. Soc.* **321**(3), 398–420 (2001) <https://doi.org/10.1046/j.1365-8711.2001.03974.x>
- [30] Guillochon, J., Ramirez-Ruiz, E., Lin, D.: Consequences of the Ejection and Disruption of Giant Planets. *Astrophys. J.* **732**(2), 74 (2011) <https://doi.org/10.1088/0004-637X/732/2/74> [arXiv:1012.2382](https://arxiv.org/abs/1012.2382) [astro-ph.EP]
- [31] Jang-Condell, H.: On the Likelihood of Planet Formation in Close Binaries. *Astrophys. J.* **799**(2), 147 (2015) <https://doi.org/10.1088/0004-637X/799/2/147> [arXiv:1501.00617](https://arxiv.org/abs/1501.00617) [astro-ph.EP]
- [32] Liu, Y., Lu, T., Rice, M.: The Formation of Double Hot Jupiter Systems through von Zeipel–Lidov–Kozai Migration. *Astrophys. J.* **986**(1), 103 (2025) <https://doi.org/10.3847/1538-4357/add405> [arXiv:2505.04398](https://arxiv.org/abs/2505.04398) [astro-ph.EP]
- [33] Beleznay, M., Kunimoto, M.: Exploring the dependence of hot Jupiter occurrence rates on stellar mass with TESS. *Mon. Not. R. Astron. Soc.* **516**(1), 75–83 (2022) <https://doi.org/10.1093/mnras/stac2179> [arXiv:2207.12522](https://arxiv.org/abs/2207.12522) [astro-ph.EP]
- [34] Gautham Bhaskar, H., Perets, H.: Properties of Free Floating Planets Ejected through Planet-Planet Scattering. *arXiv e-prints*, 2501–13166 (2025) <https://doi.org/10.48550/arXiv.2501.13166> [arXiv:2501.13166](https://arxiv.org/abs/2501.13166) [astro-ph.EP]
- [35] Hut, P.: Tidal evolution in close binary systems. *Astron. Astrophys.* **99**, 126–140 (1981)
- [36] Stegmann, J., Vigna-Gómez, A., Rantala, A., Wagg, T., Zwick, L., Renzo, M., van Son, L.A.C., de Mink, S.E., White, S.D.M.: Close Encounters of Wide Binaries Induced by the Galactic Tide: Implications for Stellar Mergers and Gravitational-wave Sources. *Astrophys. J. Lett.* **972**(2), 19 (2024) <https://doi.org/10.3847/2041-8213/ad70bb> [arXiv:2405.02912](https://arxiv.org/abs/2405.02912) [astro-ph.GA]
- [37] Tu, P.-W., Xie, J.-W., Chen, D.-C., Zhou, J.-L.: Age dependence of the occurrence and architecture of ultra-short-period planet systems. *Nature Astronomy* **9**,

995–1006 (2025) <https://doi.org/10.1038/s41550-025-02539-1> arXiv:2504.20986 [astro-ph.EP]

[38] Antognini, J.M.O.: Timescales of Kozai-Lidov oscillations at quadrupole and octupole order in the test particle limit. *Mon. Not. R. Astron. Soc.* **452**(4), 3610–3619 (2015) <https://doi.org/10.1093/mnras/stv1552> arXiv:1504.05957 [astro-ph.EP]

[39] Luo, L., Katz, B., Dong, S.: Double-averaging can fail to characterize the long-term evolution of Lidov-Kozai Cycles and derivation of an analytical correction. *Mon. Not. R. Astron. Soc.* **458**(3), 3060–3074 (2016) <https://doi.org/10.1093/mnras/stw475> arXiv:1601.04345 [astro-ph.EP]

[40] Tremaine, S.: The Hamiltonian for von Zeipel-Lidov-Kozai oscillations. *Mon. Not. R. Astron. Soc.* **522**(1), 937–947 (2023) <https://doi.org/10.1093/mnras/stad1029> arXiv:2304.01257 [astro-ph.EP]

[41] Klein, Y.Y., Katz, B.: Hierarchical three-body problem at high eccentricities = simple pendulum II: octupole including Brown’s Hamiltonian. *Mon. Not. R. Astron. Soc.* **535**(1), 31–36 (2024) <https://doi.org/10.1093/mnrasl/slae089> arXiv:2408.04003 [astro-ph.EP]

[42] Grishin, E., Perets, H.B., Fragione, G.: Quasi-secular evolution of mildly hierarchical triple systems: analytics and applications for GW sources and hot Jupiters. *Mon. Not. R. Astron. Soc.* **481**, 4907 (2018) <https://doi.org/10.1093/mnras/sty2477>

[43] Mangipudi, A., Grishin, E., Trani, A.A., Mandel, I.: Extreme Eccentricities of Triple Systems: Analytic Results. *Astrophys. J.* **934**(1), 44 (2022) <https://doi.org/10.3847/1538-4357/ac7958> arXiv:2205.08703 [astro-ph.EP]

[44] Grishin, E.: Irregular fixation: I. Fixed points and librating orbits of the Brown Hamiltonian. *Mon. Not. R. Astron. Soc.* **533**(1), 486–496 (2024) <https://doi.org/10.1093/mnras/stae1833> arXiv:2407.05122 [astro-ph.EP]

[45] Grishin, E.: Irregular Fixation II: The orbits of irregular satellites. arXiv e-prints, 2407–05123 (2024) <https://doi.org/10.48550/arXiv.2407.05123> arXiv:2407.05123 [astro-ph.EP]

[46] Lei, H., Grishin, E.: Extensions of Brown Hamiltonian - I. A high-accuracy model for von Zeipel-Lidov-Kozai oscillations. *Mon. Not. R. Astron. Soc.* **540**(3), 2422–2431 (2025) <https://doi.org/10.1093/mnras/staf843> arXiv:2505.13780 [astro-ph.EP]

[47] Lei, H., Grishin, E.: Extensions of Brown Hamiltonian-II. Analytical study on the modified von Zeipel-Lidov-Kozai effects. arXiv e-prints, 2507–11184 (2025) arXiv:2507.11184 [astro-ph.EP]

[48] Naoz, S., Farr, W.M., Lithwick, Y., Rasio, F.A., Teyssandier, J.: Secular dynamics in hierarchical three-body systems. *Mon. Not. R. Astron. Soc.* **431**(3), 2155–2171 (2013) <https://doi.org/10.1093/mnras/stt302> arXiv:1107.2414 [astro-ph.EP]

[49] Liu, B., Muñoz, D.J., Lai, D.: Suppression of extreme orbital evolution in triple systems with short-range forces. *Mon. Not. R. Astron. Soc.* **447**(1), 747–764 (2015) <https://doi.org/10.1093/mnras/stu2396> arXiv:1409.6717 [astro-ph.EP]

[50] Weldon, G.C., Naoz, S., Hansen, B.M.S.: Analytical Models for Secular Descents in Hierarchical Triple Systems. *Astrophys. J.* **974**(2), 302 (2024) <https://doi.org/10.3847/1538-4357/ad77a9> arXiv:2405.20377 [astro-ph.EP]

[51] Hamilton, C., Rafikov, R.R.: Secular dynamics of binaries in stellar clusters - II. Dynamical evolution. *Mon. Not. R. Astron. Soc.* **488**(4), 5512–5535 (2019) <https://doi.org/10.1093/mnras/stz2026> arXiv:1902.01345 [astro-ph.SR]

[52] Tremaine, S., Touma, J., Namouni, F.: Satellite Dynamics on the Laplace Surface. *Astron. J.* **137**(3), 3706–3717 (2009) <https://doi.org/10.1088/0004-6256/137/3/3706> arXiv:0809.0237 [astro-ph]

[53] Vigna-Gómez, A., Grishin, E., Stegmann, J., Olejak, A., Popa, S.A., Liu, B., Rajamuthukumar, A.S., van Son, L.A.C., Bobrick, A., Dorozsmai, A.: Prompt stellar and binary black hole mergers in tight triples: Insights from chemically homogeneous evolution. *arXiv e-prints*, 2503–17006 (2025) <https://doi.org/10.48550/arXiv.2503.17006> arXiv:2503.17006 [astro-ph.SR]

[54] Grishin, E., Perets, H.B., Zenati, Y., Michaely, E.: Generalized Hill-stability criteria for hierarchical three-body systems at arbitrary inclinations. *Mon. Not. R. Astron. Soc.* **466**(1), 276–285 (2017) <https://doi.org/10.1093/mnras/stw3096> arXiv:1609.05912 [astro-ph.EP]

[55] Tory, M., Grishin, E., Mandel, I.: Empirical stability boundary for hierarchical triples. *Publ. Astron. Soc. Aust.* **39**, 062 (2022) <https://doi.org/10.1017/pasa.2022.57> arXiv:2208.14005 [astro-ph.SR]

[56] Vynatheya, P., Hamers, A.S., Mardling, R.A., Bellinger, E.P.: Algebraic and machine learning approach to hierarchical triple-star stability. *Mon. Not. R. Astron. Soc.* **516**(3), 4146–4155 (2022) <https://doi.org/10.1093/mnras/stac2540> arXiv:2207.03151 [astro-ph.SR]

[57] Gan, T., Guo, K., Liu, B., Wang, S.X., Mao, S., Buchner, J., Fulton, B.J.: Relative Occurrence Rate between Hot and Cold Jupiters as an Indicator to Probe Planet Migration. *Astrophys. J.* **967**(1), 74 (2024) <https://doi.org/10.3847/1538-4357/ad3deb> arXiv:2404.07033 [astro-ph.EP]

[58] Gan, T., Wang, S.X., Wang, S., Mao, S., Huang, C.X., Collins, K.A., Stassun,

K.G., Shporer, A., Zhu, W., Ricker, G.R., Vanderspek, R., Latham, D.W., Seager, S., Winn, J.N., Jenkins, J.M., Barkaoui, K., Belinski, A.A., Ciardi, D.R., Evans, P., Girardin, E., Maslenikova, N.A., Mazeh, T., Panahi, A., Pozuelos, F.J., Radford, D.J., Schwarz, R.P., Twicken, J.D., Wünsche, A., Zucker, S.: Occurrence Rate of Hot Jupiters Around Early-type M Dwarfs Based on Transiting Exoplanet Survey Satellite Data. *Astron. J.* **165**(1), 17 (2023) <https://doi.org/10.3847/1538-3881/ac9b12> arXiv:2210.08313 [astro-ph.EP]

[59] Gan, T., Theissen, C.A., Wang, S.X., Burgasser, A.J., Mao, S.: Metallicity Dependence of Giant Planets around M Dwarfs. *Astrophys. J. Suppl. Ser.* **276**(2), 47 (2025) <https://doi.org/10.3847/1538-4365/ad9c65> arXiv:2412.06137 [astro-ph.EP]

[60] Torres, G., Andersen, J., Giménez, A.: Accurate masses and radii of normal stars: modern results and applications. *Astron. Astrophys. Rev.* **18**(1-2), 67–126 (2010) <https://doi.org/10.1007/s00159-009-0025-1> arXiv:0908.2624 [astro-ph.SR]

[61] Duquennoy, A., Mayor, M.: Multiplicity among Solar Type Stars in the Solar Neighbourhood - Part Two - Distribution of the Orbital Elements in an Unbiased Sample. *Astron. Astrophys.* **248**, 485 (1991)

[62] Gaia Collaboration, Brown, A.G.A., Vallenari, A., Prusti, T., de Bruijne, J.H.J., Babusiaux, C., Biermann, M., Creevey, O.L., Evans, D.W., Eyer, L., Hutton, A., Jansen, F., Jordi, C., Klioner, S.A., Lammers, U., Lindegren, L., Luri, X., Mignard, F., Panem, C., Pourbaix, D., Randich, S., Sartoretti, P., Soubiran, C., Walton, N.A., Arenou, F., Bailer-Jones, C.A.L., Bastian, U., Cropper, M., Drimmel, R., Katz, D., Lattanzi, M.G., van Leeuwen, F., Bakker, J., Cacciari, C., Castañeda, J., De Angeli, F., Ducourant, C., Fabricius, C., Fouesneau, M., Frémat, Y., Guerra, R., Guerrier, A., Guiraud, J., Jean-Antoine Piccolo, A., Masana, E., Messineo, R., Mowlavi, N., Nicolas, C., Niemartowicz, K., Pailler, F., Panuzzo, P., Riclet, F., Roux, W., Seabroke, G.M., Sordo, R., Tanga, P., Thévenin, F., Gracia-Abril, G., Portell, J., Teyssier, D., Altmann, M., Andrae, R., Bellas-Velidis, I., Benson, K., Berthier, J., Blomme, R., Brugaletta, E., Burgess, P.W., Busso, G., Carry, B., Cellino, A., Cheek, N., Clementini, G., Damerdji, Y., Davidson, M., Delchambre, L., Dell’Oro, A., Fernández-Hernández, J., Galluccio, L., García-Lario, P., Garcia-Reinaldos, M., González-Núñez, J., Gosset, E., Haigron, R., Halbwachs, J.-L., Hambley, N.C., Harrison, D.L., Hatzidimitriou, D., Heiter, U., Hernández, J., Hestroffer, D., Hodgkin, S.T., Holl, B., Janßen, K., Jevardat de Fombelle, G., Jordan, S., Krone-Martins, A., Lanzafame, A.C., Löffler, W., Lorca, A., Manteiga, M., Marchal, O., Marrese, P.M., Moitinho, A., Mora, A., Muinonen, K., Osborne, P., Pancino, E., Pauwels, T., Petit, J.-M., Recio-Blanco, A., Richards, P.J., Riello, M., Rimoldini, L., Robin, A.C., Roegiers, T., Rybizki, J., Sarro, L.M., Siopis, C., Smith, M., Sozzetti, A., Ulla, A., Utrilla, E., van Leeuwen, M., van Reeven, W., Abbas, U., Abreu Aramburu, A., Accart, S., Aerts, C., Aguado, J.J., Ajaj, M., Altavilla, G., Álvarez, M.A., Álvarez Cid-Fuentes, J., Alves, J., Anderson, R.I., Anglada Varela, E., Antoja, T.,

Audard, M., Baines, D., Baker, S.G., Balaguer-Núñez, L., Balbinot, E., Balog, Z., Barache, C., Barbato, D., Barros, M., Barstow, M.A., Bartolomé, S., Bassilana, J.-L., Bauchet, N., Baudesson-Stella, A., Becciani, U., Bellazzini, M., Bernet, M., Bertone, S., Bianchi, L., Blanco-Cuaresma, S., Boch, T., Bombrun, A., Bossini, D., Bouquillon, S., Bragaglia, A., Bramante, L., Breedt, E., Bressan, A., Brouillet, N., Bucciarelli, B., Burlacu, A., Busonero, D., Butkevich, A.G., Buzzi, R., Caffau, E., Cancelliere, R., Cánovas, H., Cantat-Gaudin, T., Carballo, R., Carlucci, T., Carnerero, M.I., Carrasco, J.M., Casamiquela, L., Castellani, M., Castro-Ginard, A., Castro Sampol, P., Chaoul, L., Charlot, P., Chemin, L., Chiavassa, A., Cioni, M.-R.L., Comoretto, G., Cooper, W.J., Cornez, T., Cowell, S., Crifo, F., Crosta, M., Crowley, C., Dafonte, C., Dapergolas, A., David, M., David, P.: Gaia Early Data Release 3. Summary of the contents and survey properties. *Astron. Astrophys.* **649**, 1 (2021) <https://doi.org/10.1051/0004-6361/202039657> [arXiv:2012.01533](https://arxiv.org/abs/2012.01533) [astro-ph.GA]

[63] Hwang, H.-C., Ting, Y.-S., Zakamska, N.L.: The eccentricity distribution of wide binaries and their individual measurements. *Mon. Not. R. Astron. Soc.* **512**(3), 3383–3399 (2022) <https://doi.org/10.1093/mnras/stac675> [arXiv:2111.01789](https://arxiv.org/abs/2111.01789) [astro-ph.SR]

[64] Hamilton, C.: On the Phase-mixed Eccentricity and Inclination Distributions of Wide Binaries in the Galaxy. *Astrophys. J. Lett.* **929**(2), 29 (2022) <https://doi.org/10.3847/2041-8213/ac6600> [arXiv:2202.01307](https://arxiv.org/abs/2202.01307) [astro-ph.GA]

[65] Moorhead, A.V., Ford, E.B., Morehead, R.C., Rowe, J., Borucki, W.J., Batalha, N.M., Bryson, S.T., Caldwell, D.A., Fabrycky, D.C., Gautier, T.N., Koch, D.G., Holman, M.J., Jenkins, J.M., Li, J., Lissauer, J.J., Lucas, P., Marcy, G.W., Quinn, S.N., Quintana, E., Ragozzine, D., Shporer, A., Still, M., Torres, G.: The distribution of transit durations for kepler planet candidates and implications for their orbital eccentricities. *The Astrophysical Journal Supplement Series* **197**(1), 1 (2011) <https://doi.org/10.1088/0067-0049/197/1/1>

[66] Christian, S., Vanderburg, A., Becker, J., Kraus, A.L., Pearce, L., Collins, K.A., Rice, M., Jensen, E.L.N., Baker, D., Bozza, V., Benni, P., Bieryla, A., Binnendifeld, A., Collins, K.I., Conti, D.M., Crossfield, I.J.M., Evans, P., Johnson, M.C., Girardin, E., Gregorio, J., Lewin, P., Mazeh, T., Murgas, F., Panahi, A., Pozuelos, F.J., Radford, D.J., Relles, H.M., Rodriguez Frustaglia, F., Schwarz, R.P., Srdoc, G., Stockdale, C., Tan, T.-G., Waalkes, W.C., Wang, G., Witrock, J., Zucker, S.: Wide Binary Orbits Are Preferentially Aligned with the Orbits of Small Planets, but Probably Not Hot Jupiters. *Astron. J.* **169**(6), 308 (2025) <https://doi.org/10.3847/1538-3881/adc933> [arXiv:2405.10379](https://arxiv.org/abs/2405.10379) [astro-ph.EP]

[67] Bashi, D., Helled, R., Zucker, S., Mordasini, C.: Two empirical regimes of the planetary mass-radius relation. *Astron. Astrophys.* **604**, 83 (2017) <https://doi.org/10.1051/0004-6361/201629922> [arXiv:1701.07654](https://arxiv.org/abs/1701.07654) [astro-ph.EP]

[68] Müller, S., Baron, J., Helled, R., Bouchy, F., Parc, L.: The mass-radius relation of exoplanets revisited. *Astron. Astrophys.* **686**, 296 (2024) <https://doi.org/10.1051/0004-6361/202348690> arXiv:2311.12593 [astro-ph.EP]

[69] Komacek, T.D., Youdin, A.N.: Structure and Evolution of Internally Heated Hot Jupiters. *Astrophys. J.* **844**(2), 94 (2017) <https://doi.org/10.3847/1538-4357/aa7b75> arXiv:1706.07605 [astro-ph.EP]

[70] Rozner, M., Glanz, H., Perets, H.B., Grishin, E.: Inflated Eccentric Migration of Evolving Gas Giants I - Accelerated Formation and Destruction of Hot and Warm Jupiters. *Astrophys. J.* **931**(1), 10 (2022) <https://doi.org/10.3847/1538-4357/ac6808> arXiv:2111.12718 [astro-ph.EP]

[71] Glanz, H., Rozner, M., Perets, H.B., Grishin, E.: Inflated Eccentric Migration of Evolving Gas Giants II - Numerical Methodology and Basic Concepts. *Astrophys. J.* **931**(1), 11 (2022) <https://doi.org/10.3847/1538-4357/ac6807> arXiv:2111.12714 [astro-ph.EP]

[72] Moe, M., Kratter, K.M.: Dynamical Formation of Close Binaries during the Pre-main-sequence Phase. *Astrophys. J.* **854**(1), 44 (2018) <https://doi.org/10.3847/1538-4357/aaa6d2> arXiv:1706.09894 [astro-ph.SR]

[73] Kaib, N.A., Raymond, S.N.: Very Wide Binary Stars as the Primary Source of Stellar Collisions in the Galaxy. *Astrophys. J.* **782**(2), 60 (2014) <https://doi.org/10.1088/0004-637X/782/2/60> arXiv:1309.3272 [astro-ph.SR]

[74] Mardling, R.A.: The Role of Chaos in the Circularization of Tidal Capture Binaries. I. The Chaos Boundary. *Astrophys. J.* **450**, 722 (1995) <https://doi.org/10.1086/176178>

[75] Mardling, R.A.: The Role of Chaos in the Circularization of Tidal Capture Binaries. II. Long-Time Evolution. *Astrophys. J.* **450**, 732 (1995) <https://doi.org/10.1086/176179>

[76] Vick, M., Lai, D.: Dynamical tides in highly eccentric binaries: chaos, dissipation, and quasi-steady state. *Mon. Not. R. Astron. Soc.* **476**(1), 482–495 (2018) <https://doi.org/10.1093/mnras/sty225> arXiv:1708.09392 [astro-ph.SR]

[77] Wu, Y.: Diffusive Tidal Evolution for Migrating Hot Jupiters. *Astron. J.* **155**(3), 118 (2018) <https://doi.org/10.3847/1538-3881/aaa970> arXiv:1710.02542 [astro-ph.EP]

[78] Vick, M., Lai, D., Anderson, K.R.: Chaotic tides in migrating gas giants: forming hot and transient warm Jupiters via Lidov-Kozai migration. *Mon. Not. R. Astron. Soc.* **484**(4), 5645–5668 (2019) <https://doi.org/10.1093/mnras/stz354> arXiv:1812.05618 [astro-ph.EP]

[79] Alvarado-Montes, J.A., Sucerquia, M., Zuluaga, J.I., Schwab, C.: Orbital Decay of the Ultra-hot Jupiter TOI-2109b: Tidal Constraints and Transit-timing Analysis. *Astrophys. J.* **988**(1), 66 (2025) <https://doi.org/10.3847/1538-4357/ade057> [arXiv:2505.18941](https://arxiv.org/abs/2505.18941) [astro-ph.EP]